BUOYANT JET MODEL TO PREDICT A VERTICAL THERMAL STRATIFICATION DURING REFUELING OF GASEOUS HYDROGEN TANKS IN HORIZONTAL POSITION WITH AXIAL INJECTION

Gonin, R.[1], Fabre, D.[2], Bourguet, R.[2], Ammouri, F.[1] and Vyazmina, E.[1]
[1]Air Liquide Innovation Campus Paris, 1 Chemin de la Porte des Loges, Les Loges-en-Josas, 78350, France, remi.gonin@airliquide.com
[2]Institut de mécanique des fluides de Toulouse (IMFT), 2 allée Camille Soula, Toulouse, 31400, France

ABSTRACT

Thermodynamic modeling of hydrogen tank refueling, i.e. 0 dimension (0D) model, considers the gas in the tank as a single homogeneous volume. Based on thermodynamic considerations, i.e. mass and energy balance equations, the gas temperature and pressure predicted at each time step are volume-averaged. These models cannot detect the onset of the thermal stratification, nor the maximum local temperature of the gas inside the tank.

For safety reasons, the temperature must be maintained below 85 °C in the composite tank. When thermal stratification occurs, the volume-averaged gas temperature predicted by 0D models can be below 85 °C while local temperature may significantly exceed 85 °C. Then, thermally stratified scenarios must be predicted to still employ 0D models safely.

Up to now, only computational fluid dynamics (CFD) approaches can predict the onset of the thermal stratification and estimate the amplitude of thermal gradients. However, CFD approaches require much larger computational resources and CPU time than 0D models. This makes it difficult to use CFD for parametric studies or a live-stream temperature prediction for embedded applications. Previous CFD studies revealed the phenomenon of jet deflection during horizontal refueling of hydrogen tanks. The cold hydrogen injected into the warm gas bulk forms a round jet sinking down towards the lower part of the tank due to buoyancy forces. The jet breaks the horizontal symmetry and dumps the cold gas towards the lower part of the tank.

The jet behavior is a key factor for the onset of the thermal stratification for horizontally filled tanks. Free round jets released in a homogeneous environment with a different density than the jet density were extensively investigated in the literature. A buoyant round jet modeling can be applied to predict the jet deflection in the tank. It requires initial conditions that can be provided by 0D refueling models. Therefore, 0D models coupled with a buoyant round jet modeling can be used to predict the onset of the thermal stratification without CFD simulation. This approach clarifies the validity domain of 0D models, and thus improves the safety of engineering applications

1.0 INTRODUCTION

As presented in the last Intergovernmental Panel on Climate Change (IPCC) report [1], human activities are responsible for an increase of the global temperature of 1.1°C compared with temperatures during the pre-industrial area, principally due to greenhouse gases emissions. Thanks to its ability to generate electricity via a fuel cell without CO2 emissions, hydrogen when produced with renewable sources, appears as an interesting energy carrier to help decarbonizing the mobility industry.
For mobility application, the hydrogen is mostly used in a gaseous state stored at high pressure. Refueling protocols have been designed to safely used hydrogen as fuel to power light-duty [2] and heavy-duty vehicles [3]. A maximum of embedded mass of hydrogen is desirable to improve the driving range. Then, the nominal working pressure in the tank can reach 700 bar to obtain a density about 40 kg/m^3 at standard temperature (15 °C).

During refueling of hydrogen tanks, due to the gas compression, the gas temperature will rise. As recommended in the J2601 standard from the Society of Automotive Engineers (SAE) [4], at any time, the temperature in the tank must be kept between -40 °C and 85 °C. Consequently, the temperature in the gas during the refueling process must be controlled. The temperature at the end of a refueling is a result of different factors:

- The temperature of the injected hydrogen: The final temperature is impacted by the injected temperature [5]. To limit the rise of the temperature, the injected temperature can be cooled down to -40 °C.
- The tank materials: Generally, a type III and type IV tanks are used when the pressure is reaching 700 bar. Type III has a metallic liner whereas plastic liner is used in type IV. The thermal conductivity of walls plays a key role in the heat exchanged by the gas with the ambient environment.
- The refueling time: The total heat exchanged by the gas with walls depends on the refueling time [6-8].
- The injection velocity: The total heat exchanged by the gas with walls depends on gas velocities in the tank due to the heat transferred by convection. The gas velocities in the tank depend on the injection velocity.

Taking into account all above, to predict the gas temperature at the end of the refueling, 0D models have been widely developed in the literature [9-13]. Based on thermodynamical considerations, i.e. mass and energy balance equations, applied to the total volume of the gas, 0D models can predict volume-averaged thermodynamical properties in the gas.
This gives a uniform gas temperature, pressure and density during the refueling. The advantage of this numerical approach is to allow rapid calculation of tank refueling, i.e. some minutes on a laptop computer. With this numerical approach, the injection temperature can be estimated rapidly in order to avoid having an average gas temperature over 85 °C at the end of the refueling.

The limit of this approach is to not consider thermal heterogeneities during the refueling, i.e. situations where local gas temperatures differ substantially from the gas average temperature. However, refueling scenarios leading to thermal heterogeneities exist.
Merida et al. [6] experimentally found a link between the thermal heterogeneity of the tank and the refueling mass flowrate. The injection velocity is responsible for the thermal mixing of the gas inside the tank. Terada et al. [14] found that for a type IV 65 L tank filled until 350 bar, a vertical thermal gradient is occurring when the injection velocity is below 5 m/s.
This criterion was confirmed for a type IV 36 L tank and a type III 40 L tank during HyTransfer project [15,16]. Using different injectors and mass flowrates, it was demonstrated that a vertical thermal gradient occurs when the injection velocity is below 5 m/s.
Nowadays, the CFD approach is the only numerical approach able to predict the onset of the thermal stratification [17-20,23]. This numerical approach can take into account the three-dimensions nature of the flow, which is essential to capture the thermal heterogeneities in the gas.
However, the CFD approach requires large computational resources. Hence, this approach cannot be used for engineering application such as real-time temperature predictions or large-range parametrical studies.
Up to now, only the Terada criterion [14] is available to predict vertical thermal stratifications: velocity of the gas at the injector must be maintain above 5 m/s to avoid vertical thermal stratification. It is an empirical criterion. When the refueling conditions are far from the experimental conditions of Terada, for instance, tanks with larger aspect ratio (inner length over inner diameter, L/D>3) or gases different from hydrogen, the Terada criterion cannot to be applied.

The objective of this study is to suggest a criterion that predicts the onset of the thermal stratification for horizontally filled tank based on physical considerations. By using the buoyant round jet theory [21], a jet trajectory model is developed. From this model, a dimensionless Froude number is constructed, equal to 1 when vertical thermal stratification occurs. This Froude number can be calculated with data from 0D models or measured data.

2.0 PHYSICAL SYSTEM DESCRIPTION

The refueling of a hydrogen tank consists in injecting a mass of hydrogen inside a closed volume. The increase of the mass of the gas in a constant volume induces a rise of the gas pressure and the temperature due to the compression.
Fig. 1 presents a tank geometry configuration. The tank has a circular symmetry around its main axis, the x-axis. The hydrogen is injected via an injector device, the pipe.
This study concerns tanks laying in horizontal position with a pipe injecting axially the gas, i.e. along the x-axis. The gravity $\vec{g}$ is pointing along the y-axis.
In this study, the origin of the coordinate system is taken at the pipe outlet.
The tank real geometry is approximated and is considered as a perfect cylinder. The internal radius of the tank is named R_{tank} $[m]$ and the internal length of the tank is named L_{tank} $[m]$.
The pipe is considered cylindrical. Its length is named L_{inj} $[m]$ and its the inner radius is named r_0 $[m]$.

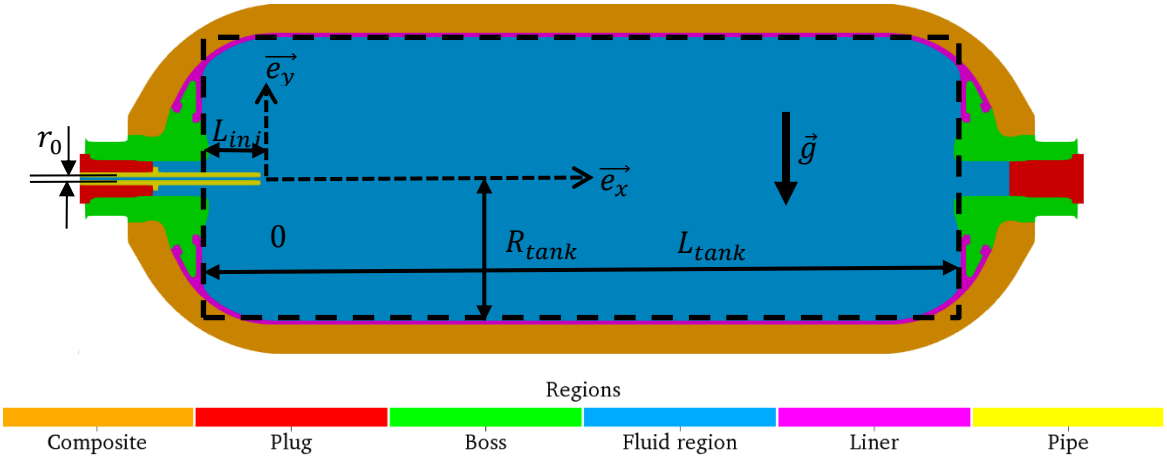

Figure 1. Scheme of a hydrogen tank. View through the plane (x,y). Main geometrical lengths are reported onto the scheme.

3.0 BUOYANT JET MODEL

The buoyant jet model is used for many applications, e.g. to model a discharge of wastewater into the receiving water bodies or to model smokestacks [21]. This study aims to apply this model to the refueling of hydrogen tanks. Despite the bounded nature of the environment surrounding the jet (presence of the tank walls), the model is able to give insights on the jet trajectory inside the tank and this allows predicting the onset of the thermal stratification.
Only the essential information concerning the model is presented in this study. More details concerning the buoyant jet model can be found in [21].
As presented in Fig. 2, the reference frame is a fixed Cartesian coordinate system $(\overrightarrow{e_x}, \overrightarrow{e_y}, \overrightarrow{e_z})$. A local cylindrical coordinate system $(\overrightarrow{e_s}, \overrightarrow{e_r}, \overrightarrow{e_z})$ is set to follow the jet centerline, described by a curvilinear abscissa s $[m]$. The pipe outlet is the origin of the coordinate system, i.e. $s = 0\ m$. The jet radius is named b [m] and is equal to r_0 $[m]$ at the origin. The jet deviation angle θ [rad] measures the angle between the x-axis and the jet trajectory.

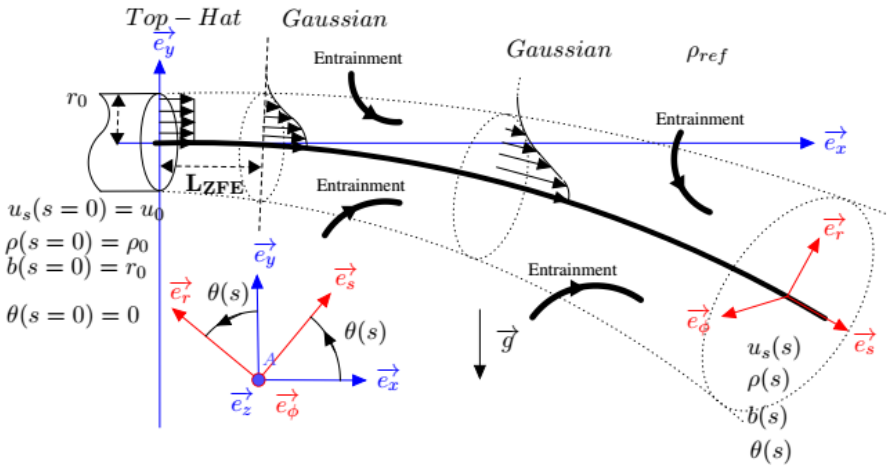

Figure 2. Scheme of the buoyant jet model. Coordinate systems and local variables are reported onto the scheme.

The injection pipe is cylindrical and then the hydrogen released at the pipe outlet is assumed to be a round jet, i.e. circular-symmetric along the x-axis. The flow is assumed turbulent at the outlet and then a uniform velocity value u_0 $[m/s]$ and density ρ_0 $[kg/m^3]$ is assumed at the pipe outlet. In the tank, out of the jet, the gas is considered at rest, i.e. no velocity, and all properties are considered uniform. The density ρ_{ref} $[kg/m^3]$ is a reference density.

The buoyant jet model is constructed using balance equations of mass, momentum and buoyancy flux (divided by the reference density), Q $[m^3/s]$, M $[m^2/s^2]$ and J $[m^2/s^2]$ respectively, applied to a plane perpendicular to the jet curvilinear abscissa. Then the mass, momentum and buoyancy flux can be defined as:

$$\mathrm{Q} = \int_0^{2\pi}\int_0^{+\infty} u_s r dr d\phi\,, \tag{1}$$

$$\mathrm{M} = \int_0^{2\pi}\int_0^{+\infty} u_s^2 r dr d\phi, \tag{2}$$

$$\mathrm{J} = \int_0^{2\pi}\int_0^{+\infty} g' u_s r dr d\phi\,. \tag{3}$$

As presented in Fig. 2, for a released jet, two area can be identified: a transition area called Zone of Flow Establishment (ZFE) [22] followed by an established flow area where the jet is assumed self-similar.

At the origin, starting point of the ZFE, the velocity and density profiles are assumed to be uniform, then:

$$\begin{cases} Q(0) = \pi u_0 r_0^2 \\ M(0) = \pi u_0^2 r_0^2 \end{cases}. \tag{4}$$

The length of the ZFE, L_{ZFE} $[m]$, is found proportional to the pipe radius [22],

$$L_{ZFE} = 9.79\, r_0. \tag{5}$$

The mass fluxes at the beginning and at the end of the ZFE are linked [22],

$$\mathrm{Q}(ZFE) = 1.72\, Q(0). \tag{6}$$

In the ZFE, the momentum flux decreasing is assumed negligible,

$$M(ZFE) = M(0)\,. \tag{7}$$

After the ZFE, a Gaussian profile is established for the velocity and density radial distributions. A dimensionless parameter λ [1] is introduced to allow different variances between the velocity and density Gaussian profiles. A reduced gravity g' [m/s^2] is introduced,

$$g' = \frac{\rho_{ref} - \rho(s)}{\rho_{ref}} g, \tag{8}$$

and then

$$\begin{cases} g'(s,r) = g_c(s)e^{-\left(\frac{r}{\lambda b}\right)^2} \\ u_s(s,r) = u_c(s)e^{-\left(\frac{r}{b}\right)^2} \end{cases}, \quad (9)$$

with $g_c\ [m/s^2]$ and $u_c\ [m/s]$, the reduced gravity and the velocity at the jet centerline.

After the ZFE, using equations (1), (2), (3) and (9), the link between local variables and integral variables can be found:

$$\begin{cases} Q = \pi b^2 u_c \\ M = \frac{1}{2}\pi b^2 u_c^2 \\ J = \frac{\lambda^2}{1+\lambda^2}\pi b^2 u_c g_c \end{cases}. \quad (10)$$

Mass balance equation applied to a plane perpendicular to the jet centerline allows linking the growth of mass flow with the entrained mass. The entrained mass is modeled using a mass entrainment rate α [1], the velocity at the jet centerline and the jet width,

$$\frac{dQ}{ds} = 2\pi b u_c \alpha, \quad (11)$$

A buoyant jet transits between two opposite behaviors: a pure jet behavior, where the flow is driven by the momentum and a pure plume behavior where the flow is driven by the natural convection. The typical mass entrainment rate for a pure jet is $\alpha = 0.055$ [21] while for a pure plume it is $\alpha = 0.083$ [21].

Momentum balance equations applied to a plane perpendicular to the jet centerline allows completing the equations system describing the jet trajectory:

$$\begin{cases} \frac{dQ}{ds} = (8\pi M)^{1/2}\alpha \\ \frac{dM}{ds} = (\lambda^2+1)\frac{JQ}{2M}\sin(\theta) \\ \frac{dJ}{ds} = 0 \\ \frac{d\theta}{ds} = (\lambda^2+1)\frac{JQ}{2M^2}\cos(\theta) \\ \frac{dx}{ds} = \cos(\theta) \\ \frac{dy}{ds} = \sin(\theta) \end{cases}, \quad (12)$$

with as initial conditions,

$$\begin{cases} Q(L_{LFE}) = 1.72\pi r_0^2 u_0 \\ M(L_{LFE}) = \pi r_0^2 u_0^2 \\ J(L_{LFE}) = \frac{\lambda^2}{1+\lambda^2}Q(L_{LFE})\frac{\rho_{ref}-\rho_0}{\rho_{ref}}g \\ \theta(L_{LFE}) = 0 \\ x(L_{LFE}) = L_{ZFE} = 9.79\, r_0 \\ y(L_{LFE}) = 0 \end{cases}. \quad (13)$$

Previous CFD simulations [17, 23] have shown that the jet deflection is a key factor of the vertical thermal stratification. The vertical thermal stratification appears when the jet is so deflected due to buoyancy forces that it hits the lower part of the tank. Simulations [17, 23] have shown that, at this instant of the refueling, the oscillations of the jet are negligible and its trajectory remains deflected toward lower part of the tank. This breaks the horizontal symmetry and favors the cooling of the lower part of the tank to the detriment of the upper part of the tank. Fig. 3 presents CFD results issued from [23]. The upper frame shows that velocity streamlines remain into the lower part of the tank. The lower frame shows that a vertical thermal stratification occurs.

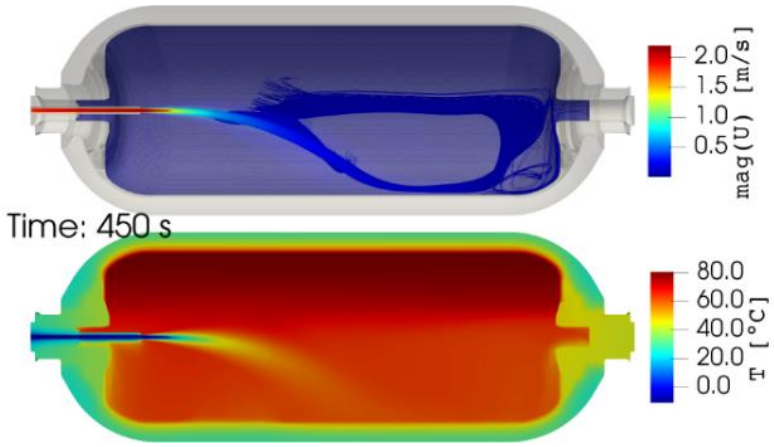

Figure 3. CFD results with a presence of vertical thermal stratification issued from [23]. The upper frame presents the velocity streamlines while the lower frame presents the thermal field.

The beginning of the thermal stratification corresponds to the moment when the jet trajectory hits this lower part of the tank. The impact coordinates are:

$$\begin{cases} x = L_{tank} - L_{inj} \\ y = -R_{tank} \end{cases}. \quad (14)$$

The equations system (12) does not admit a simple analytic solution able to link x and y. Some assumptions are performed to simplify the equations system (12). The jet deviation angle θ is assumed small enough to linearize the sine and cosine functions. Consistent with the hypothesis of a small jet deviation angle, the gain of momentum due to the negative buoyancy is assumed negligible compared to the jet inertia. Then, the equation system (12) can be reduced to

$$\begin{cases} \frac{dQ}{ds} = (8\pi M)^{\frac{1}{2}}\alpha \\ \frac{dM}{ds} = 0 \\ \frac{dJ}{ds} = 0 \\ \frac{d\theta}{ds} = (\lambda^2+1)\frac{JQ}{2M^2} \\ x = s \\ y = \theta \end{cases}. \quad (15)$$

The equation system (15) can be integrated analytically, and then it links x and y,

$$y = (\lambda^2+1)\frac{J(L_{ZFE})}{2M(L_{ZFE})^2}(x - L_{ZFE})\,[Q(L_{ZFE}) + 4\pi M^{\frac{1}{2}}\alpha(x - L_{ZFE})]. \quad (16)$$

At the impact point given in (14), using the initial conditions (13) and by introducing the reduced length $\tilde{L}$ $[m]$ defined as

$$\tilde{L} = L_{tank} - L_{inj} - L_{ZFE}, \quad (17)$$

the equation (16) can be written such as,

$$R_{tank} = (\lambda^2+1)\frac{\rho_{ref}-\rho_0}{\rho_{ref}}\frac{g\tilde{L}^2}{u_0^2}\left(0.37 + 0.23\frac{\tilde{L}}{r_0}\alpha\right). \quad (18)$$

The equation (18) can be rearranged to obtain a Froude number:

$$Fr = \frac{u_0}{\sqrt{(\lambda^2+1)\frac{\rho_{ref}-\rho_0}{\rho_{ref}}g\frac{\tilde{L}^2}{R_{tank}}\left(0.37+0.23\frac{\tilde{L}}{r_0}\alpha\right)}}. \quad (19)$$

When the jet impacts the lower part of the tank, i.e. at beginning of the vertical thermal stratification, the Froude number defined equation (19) equals 1.

It has been found that with $\alpha = 0.055$ and $\lambda = 1$, the jet trajectory given by the buoyant jet model and previous CFD results [17, 23] are in good agreement. Then (19) is simplified to

$$Fr = \frac{u_0}{\sqrt{\frac{\rho_{ref}-\rho_0}{\rho_{ref}}g\frac{\tilde{L}^2}{R_{tank}}\left(0.74+0.0223\frac{\tilde{L}}{r_0}\right)}}. \quad (20)$$

4.0 MATERIAL FOR VALIDATION

To perform the validation of the Froude number defined equation (20), experimental data from two sources [14, 15] are used.
Terada et al. [14] detected the thermal stratification for a type IV 65 L tank during a 600 s refueling scenario from 2 MPa to 35 MPa using an axial injector of 10 mm. Terada found that for this refueling configuration, when the injection velocity is below 5 m/s, the thermal stratification occurs.
To perform the buoyant jet model, the average temperature of the gas T_{av} $[°C]$ is approximated using the temperature from the probe T2, see Fig. 4, D). A pressure probe allows obtaining an average pressure p_{av} $[MPa]$ in the gas. The temperature probe T4 allows detecting when thermal stratification occurs.
In the European funded project HyTransfer [15], for three different tanks, refueling scenarios leading to thermal gradient occurrences were identified and reported in [24]. In table 1, the three tanks properties are listed.

Table 1. List of the tanks used during the HyTransfer project [15] with their geometrical and material specificities. The different experimenters were the Joint Research Centre to the European Commision (JRC), Energie Technologie (ET) and Air Liquide Advanced Technologies (ALAT).

Type	Volume [L]	Ratio L/D
III	40	2.7
IV	36.7	2.4
IV	531	5.6

For the type IV 36 L tank, using ALAT measurements, 10 temperature probes were installed in the gas volume. This allows detecting precisely the presence of thermal gradients. Six refueling scenarios, leading to different level of thermal stratifications, are selected in this study. The probe locations are shown in Fig. 4, frame B).
For the type III 40 L tank, using EC measurements, 6 temperature probes were installed in the gas volume. Two refueling scenarios are selected in this study: one leading to a homogeneous thermal behavior and one leading to a thermally stratified behavior. Type III tank uses a metallic liner, which is a good thermally conductive material. Then, for this tank, the thermal stratification in the gas was detected earlier via temperature probes set at the interface between the liner and the composite wrap than with the temperature probes in the gas. The probe locations are shown in Fig. 4, A).
For the type IV 531 L tank, using ALAT measurements, 5 temperature probes were installed in the gas volume at the rear tank area. Due to those scarce locations of gas probes, the thermal stratification occurrence in the gas was detected earlier via the temperature probes set at the interface between the liner and the composite wrap than with temperature probes in the gas. Four refueling scenarios are selected: two leading to a homogeneous thermal behavior and two leading to a thermally stratified behavior. The probe locations are shown in Fig. 4, C).
For all HyTransfer refueling scenarios considered, the average gas temperature T_{av} $[°C]$ is obtained by an arithmetical averaging of the gas temperature probes. The minimal and maximal temperature measured in the gas are named as T_{min} $[°C]$ and T_{max} $[°C]$. The pressure measured in the tank is taken as the average pressure p_{av} $[MPa]$. For probes at the interface between the liner and the composite wrap, arithmetical averages of the uppermost probes $T_{l-c\,avSup}$ $[°C]$, all probes $T_{l-c\,av}$ $[°C]$, and the lowermost probes $T_{l-c\,avInf}$ $[°C]$ are performed to detect the thermal stratification from wall temperatures. The reference density ρ_{ref} and density at the pipe outlet ρ_0 are calculated using the real gas density of hydrogen using coolProp [25]. The average temperature and pressure in the gas are used to calculate the reference density,

$$\rho_{ref} = \rho(T_{av}, p_{av}), \tag{21}$$

the injection temperature and the average pressure in the gas, $T_{injection}$ $[°C]$ and p_{av} $[MPa]$ respectively, are used to calculate the density at the pipe outlet,

$$\rho_0 = \rho\left(T_{injection}, p_{av}\right). \tag{22}$$

To obtain the velocity at the pipe outlet, the mass flowrate at the injection, named $\dot{m}$ $[kg/s]$, is needed. The mass flowrate can be approximated using time-evolution of the average density, which multiplied by the tank volume V_{tank} $[m^3]$, leads to

$$\dot{m} = V_{tank} \frac{\Delta \rho_{ref}}{\Delta t}. \quad (23)$$

Then the velocity can be deduced,

$$u_0 = \frac{\dot{m}}{\pi r_0^2 \rho_0}. \quad (24)$$

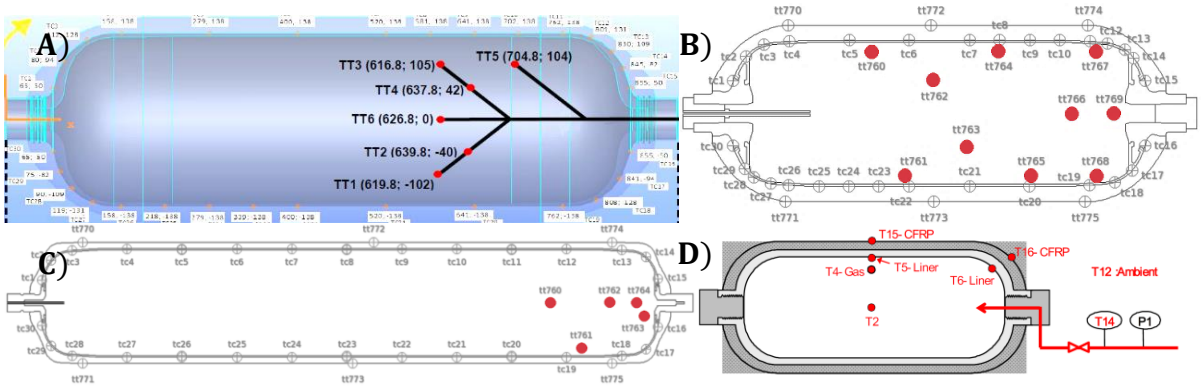

Figure 4. Probe locations from the 4 selected tanks: A) type III 40 L tank, B) type IV 36 L tank, C) type IV 531 L tank, D) type IV 65 L tank.

5.0 RESULTS

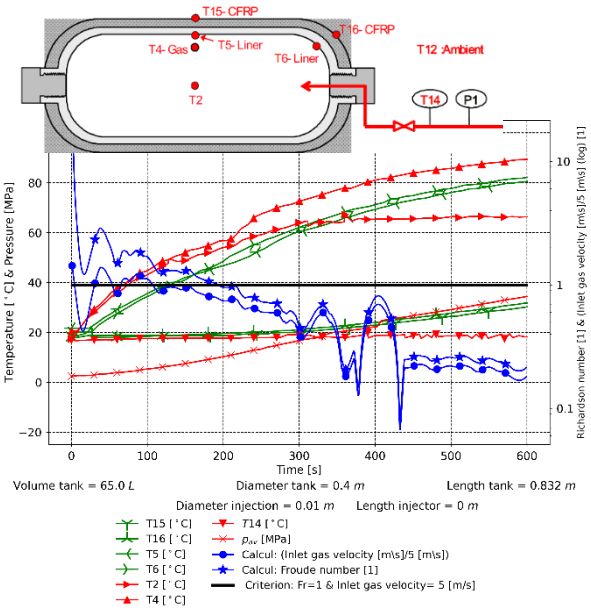

Figure 5. Data from Terada et al. [14]: type IV 65 L tank. The velocity at the pipe outlet divided by 5 m/s is reported in blue with a "bullet" marker. The Froude number defined equation (20) is reported in blue with a "star" marker. The tank and injector geometrical properties are reported above the legend of the figure.

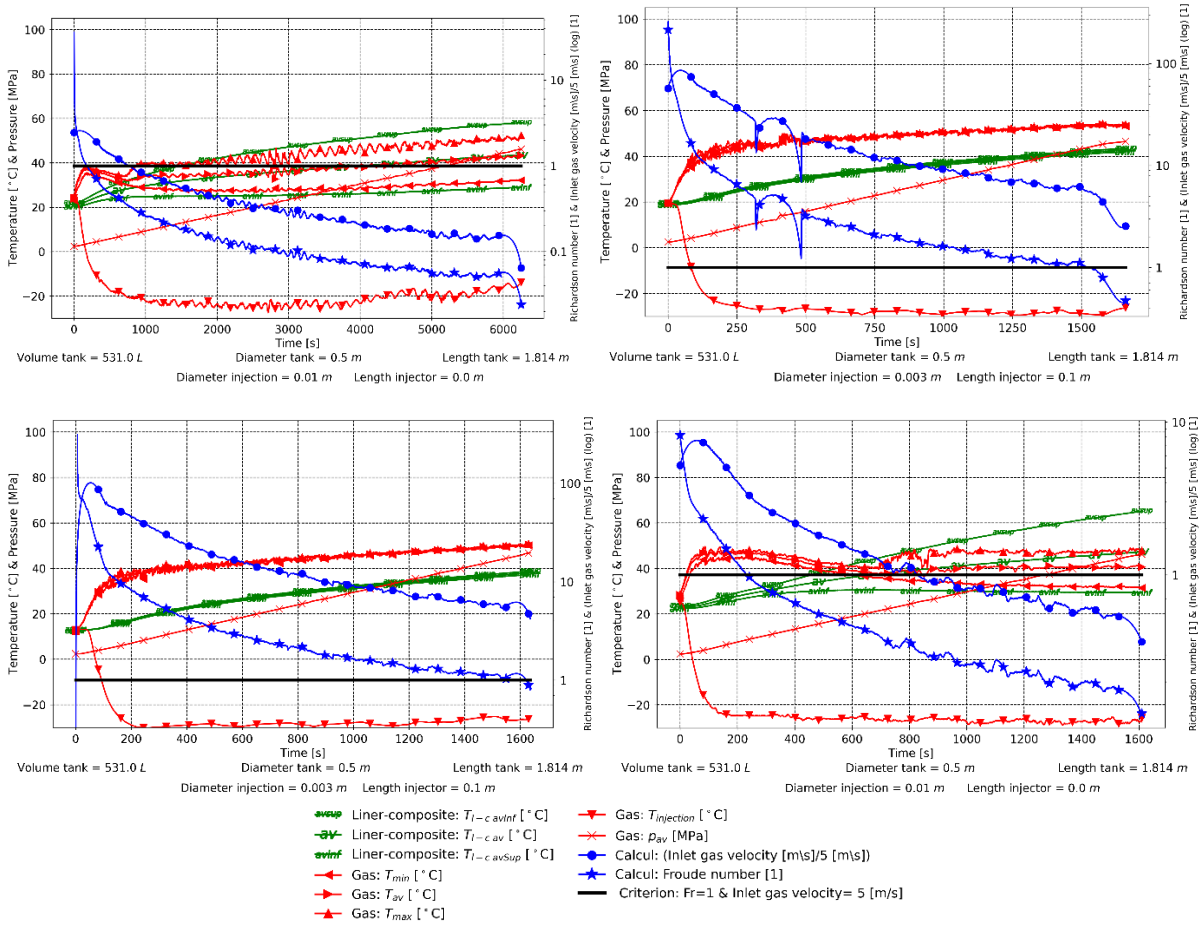

Figure 6. Data from HyTransfer [24]: type IV 531 L tank. The velocity at the pipe outlet divided by 5 m/s is reported in blue with a “bullet” marker. The Froude number defined equation (20) is reported in blue with a “star” marker. The tank and injector geometrical properties are reported above the legend of the figure.

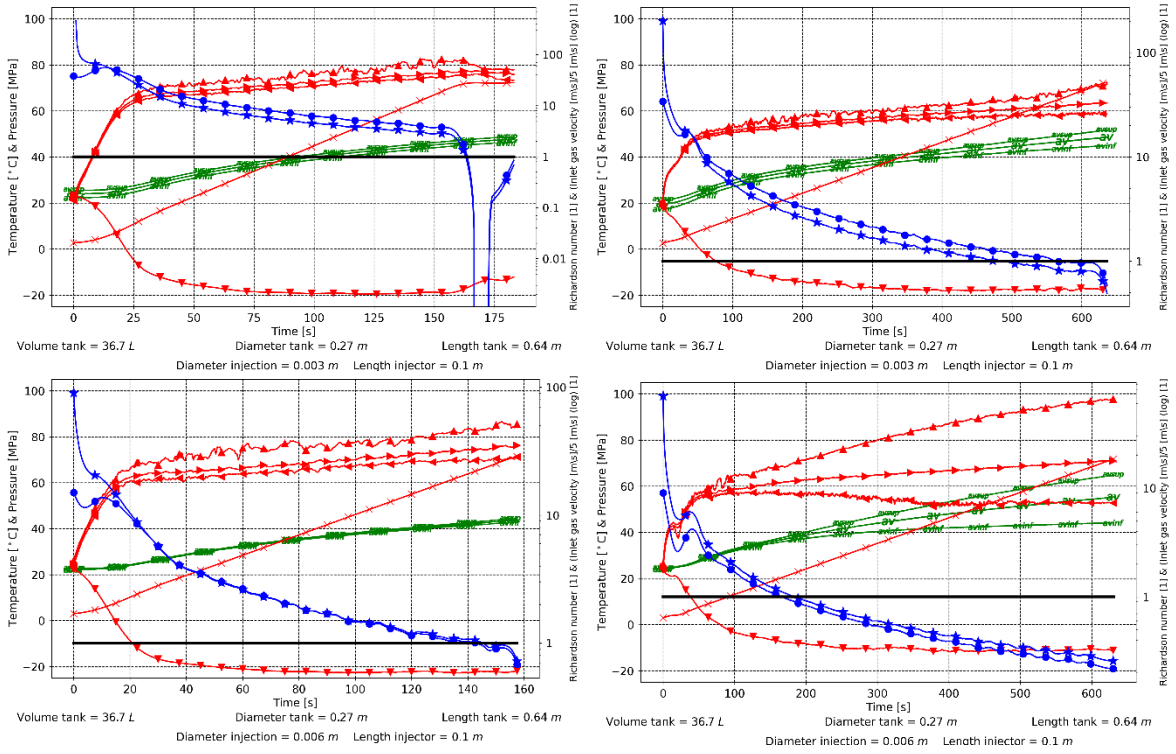

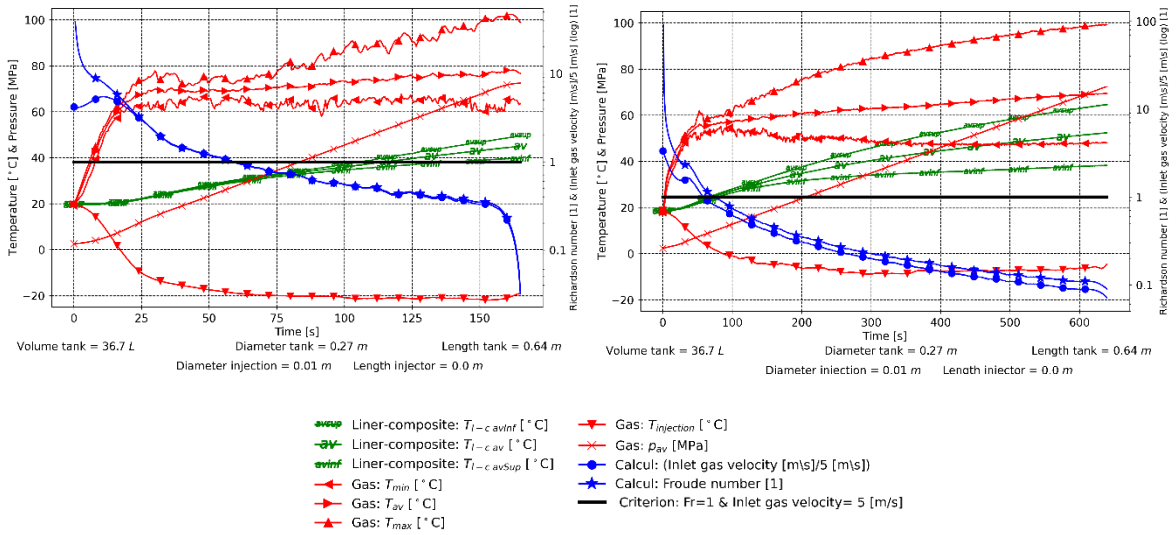

Figure 7. Data from HyTransfer [24]: type IV 36 L tank. The velocity at the pipe outlet divided by 5 m/s is reported in blue with a "bullet" marker. The Froude number defined equation (20) is reported in blue with a "star" marker. The tank and injector geometrical properties are reported above the legend of the figure.

Fig. 5, 7 and 8 show that the criterion of Terada [14] and from equation (20) are similar for small aspect ratio tanks (L/D<3). Hence, it can be seen that when $Fr = 1$ or when $u_0 = 5\,m/s$ a vertical thermal stratification occurs. In Fig. 8, the vertical thermal stratification is visible earlier from the probes located at the interface between the liner and the composite wrap (in green) than from probes located in the gas (in red) due to the metallic liner.

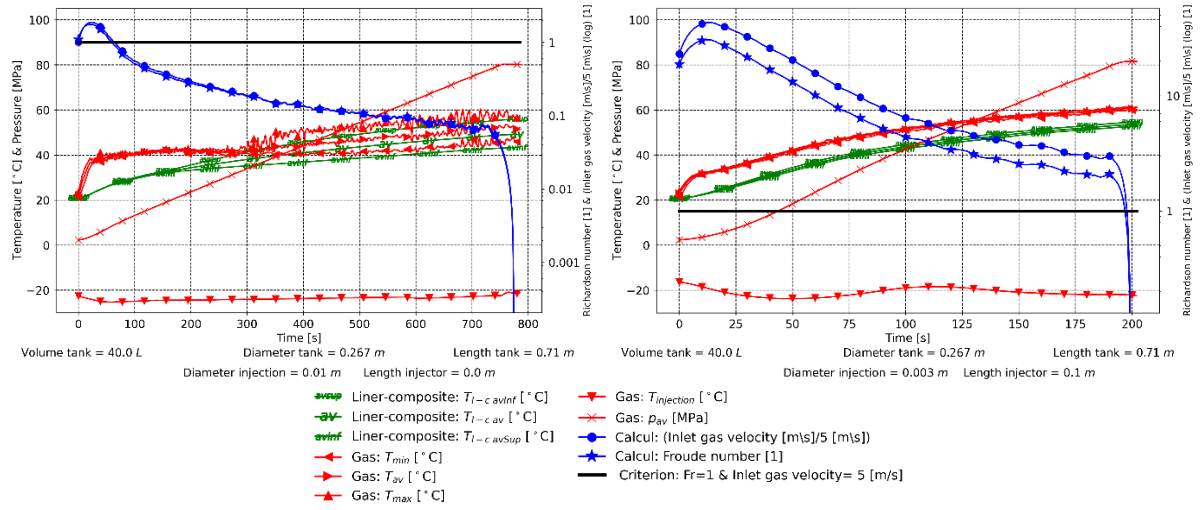

Figure 8. Data from HyTransfer [24]: type III 40 L tank. The velocity at the pipe outlet divided by 5 m/s is reported in blue with a "bullet" marker. The Froude number defined equation (20) is reported in blue with a "star" marker. The tank and injector geometrical properties are reported on above the legend of the figure.

Thermal gradients in walls are a direct consequence of thermal gradients in the gas. Since the temperature probes at the interface between the liner and the composite wrap (in green) detected a vertical thermal stratification before probes in the gas (in red), it can be assumed that the vertical thermal

stratification occurred even earlier in the gas. Then, Fig. 6 shows that the criterion $Fr = 1$ is more efficient for detecting the occurrence of thermal stratifications for a tank with a larger aspect ratio (L/D>3) than the criterion of Terada [14].

6.0 CONCLUSION

To conclude, this study suggests a new criterion which predicts the thermal stratification for horizontal tank filled axially according to the refueling conditions. It is defined via a dimensionless Froude number, see equation (20).

Experimental data concerning different tanks and refueling scenarios are used for its validation. This new criterion takes into account the gas properties and the dimensions of the tank and the pipe injector. It appears more efficient for larger aspect ratio tanks (L/D>3) than Terada [14] criterion to detect the occurrence of thermal gradients in the gas.

0D models are limited when thermal heterogeneities occur in the gas because they can only predict an average gas temperature. The Froude number defined in equation (20) can be evaluated with results from 0D models to control whether the thermal behavior in the gas is homogeneous and thus, whether the average temperature predicted in the gas is representative of temperatures in the gas.

A longer refueling time reduces the final temperature in the gas. Hence, it can be tempting to save precooling energy by reducing the mass flowrate. However, limiting the mass flowrate can lead to vertical thermal stratifications and difficulties to estimate gas temperatures without a CFD approach.
The Froude number coupled to a 0D model could help designing a low energy and safe refueling protocol for vehicles or for hydrogen tube trailers. The refueling time could be safely reduced in order to use less pre-cooling for the injected gas.

7.0 REFERENCES

1. Lee, H., K. Calvin, D. Dasgupta, G. Krinner, A. Mukherji, P. Thorne, C. Trisos, J. Romero, P. Aldunce, K. Barrett, G. Blanco, W.W.L. Cheung, S.L. Connors, F. Denton, A. Diongue-Niang, D. Dodman, M. Garschagen, O. Geden, B. Hayward, C. Jones, F. Jotzo, T. Krug, R. Lasco, J.-Y. Lee, V. Masson-Delmotte, M. Meinshausen, K. Mintenbeck, A. Mokssit, F.E.L. Otto, M. Pathak, A. Pirani, E. Poloczanska, H.-O. Pörtner, A. Revi, D.C. Roberts, J. Roy, A.C. Ruane, J. Skea, P.R. Shukla, R. Slade, A. Slangen, Y. Sokona, A.A. Sörensson, M. Tignor, D. van Vuuren, Y.-M. Wei, H. Winkler, P. Zhai, and Z. Zommers, Synthesis Report of the IPCC Sixth Assessment Report (AR6): Summary for Policymakers, Intergovernmental Panel on Climate Change, 2023.
2. Reddi, K., Elgowainy, A., Rustagi, N., and Gupta, E., Impact of hydrogen SAE J2601 fueling methods on fueling time of light-duty fuel cell electric vehicles, *International Journal of Hydrogen Energy*, **42**, Nº 26, 2017, p. 16675-16685.
3. Nouvelot, Q., Karzel, P., Hart, N., Vyazmina, E., Mattelaer, V., Sinding, C.D. and Ruiz, A., Performance metrics for refuelling protocols for heavy duty hydrogen vehicules. FCH-04-2-2019: Refuelling Protocols for Medium and Heavy-Duty Vehicules, 2020.
4. SAE International, J2601, Fueling protocols for light duty gaseous hydrogen surface vehicles. 2014.
5. Kang, Y., Cho, S. M., and Kim, D. K., Charging strategy through analysis of charging influence factors of ultra-light hydrogen storage with polyethylene terephthalate liner, *International Journal of Hydrogen Energy*, **46,** N°13, 2021, p. 9174-9185.
6. Dicken, C. J. B. and Mérida, W., Measured effects of filling time and initial mass on the temperature distribution within a hydrogen cylinder during refuelling, *Journal of Power Sources*, **165**, Nº 1, 2007, p. 324-336.
7. Wang, G., Zhou, J., Hu, S., Dong, S. and Wei, P. Investigations of filling mass with the dependence of heat transfer during fast filling of hydrogen cylinders, *International Journal of Hydrogen Energy*, **39**, Nº 9, 2014, p. 4380-4388.

8. Oh, S. J., Yoon, J. H., Jeon, K. S. and Choi, J., A study on the thermal characteristics of hydrogen storage vessel related to condition of charging, *J Mech Sci Technol*, **36**, Nº 3, 2022, p. 1579-1586.
9. Kuroki, T., Nagasawa, K., Peters, M., Leighton, D., Kurtz, J., Sakoda, N., Monde, M., Takata, Y., Thermodynamic modeling of hydrogen fueling process from high-pressure storage tank to vehicle tank, *International Journal of Hydrogen Energy*, **46**, Nº 42, 2021, p. 22004-22017.
10. Xu, Z., Dong, W., Zhao, Y., Dong, H. and He, G., Development of fuelling protocols for gaseous hydrogen vehicles: a key component for efficient and safe hydrogen mobility infrastructures, *Clean Energy*, **7**, Nº 1, 2023, p. 23-29.
11. Bourgeois, T., Ammouri, F., Baraldi, D. and Moretto, P., The temperature evolution in compressed gas filling processes: A review, *International Journal of Hydrogen Energy*, **43**, Nº 4, 2018, p. 2268-2292.
12. Bourgeois, T., Brachmann, T., Barth, F., Ammouri, F., Baraldi, D., Melideo, D., Acosta-Iborra, B., Zaepffel, D., Saury, D. and Lemonnier, D., Optimization of hydrogen vehicle refuelling requirements, *International Journal of Hydrogen Energy*, **42**, Nº 19, 2017, p. 13789-13809.
13. Molkov, V., Dadashzadeh, M. and Makarov, D., Physical model of onboard hydrogen storage tank thermal behaviour during fuelling, *International Journal of Hydrogen Energy*, **44**, Nº 8, 2019, p. 4374-4384.
14. Terada, T., Yoshimura, H., Tamura, Y., Mitsuishi, H. and Watanabe, S., Thermal behavior in hydrogen storage tank for fcv on fast filling (2nd report), SAE World Congress & Exhibition, 2008, p. 2008-01-0463.
15. HyTransfer, *European project for pre-normative research on gaseous hydrogen transfer*. 2013-2017, Funded under FP7-JTI.
16. Bourgeois, T., Ammouri, F., Baraldi, D., and Moretto, P., The temperature evolution in compressed gas filling processes: A review, *International Journal of Hydrogen Energy*, **43**, Nº 4, 2018, p. 2268-2292.
17. Gonin, R., Horgue, P., Guibert, R., Fabre, D., Bourguet, R., Ammouri, F. and Vyazmina, E., A computational fluid dynamic study of the filling of a gaseous hydrogen tank under two contrasted scenarios, *International Journal of Hydrogen Energy*, **47**, Nº 55, 2022, p. 23278-23292.
18. Li, J.-Q., Li, J.-C., Kwon, J.-T. and Shang, C., The effect of internal pressure change on the temperature rise and the amount of filling hydrogen of high pressure storage tank, *Advances in Mechanical Engineering*, **14**, Nº 8, 2022, p. 168781322211210.
19. Melideo, D., Baraldi, D., De Miguel Echevarria, N. and Acosta Iborra, B., Effects of some key-parameters on the thermal stratification in hydrogen tanks during the filling process, *International Journal of Hydrogen Energy*, **44**, Nº 26, 2019, p. 13569-13582.
20. Carrere, P., Lodier, G., Vyazmina, E., Ammouri, F., Charolais, A. and Gonin R., CFD simulations of the refueling of long horizontal H2 tanks, 9th International Conference on Hydrogen Safety (ICHS 2021), 2021.
21. Jirka, G. H., Integral Model for Turbulent Buoyant Jets in Unbounded Stratified Flows. Part I: Single Round Jet. Environmental Fluid Mechanics 4, 1–56, 2004.
22. Rajaratnam, N., Turbulent Jets, Developments in Water Science, Volume 5, Elsevier Science, 1976.
23. Gonin, R., Horgue, P., Guibert, R., Fabre, D., Bourguet, R., Ammouri, F. and Vyazmina, E., Advanced turbulence modeling improves thermal gradient prediction during compressed hydrogen tank filling, *International Journal of Hydrogen Energy*, 2023.
24. Ravinel, B., Acosta, B., De Miguel, N., Moretto, P., Ortiz-Cebolla, R., Janovic, G. and van de Löcht, U., D4.1 Report on the experimental filling test campaign, 2017.
25. Bell, I. H., Wronski, J., Quoilin, S. and Lemort, V., Pure and Pseudo-pure Fluid Thermophysical Property Evaluation and the Open-Source Thermophysical Property Library CoolProp, *Ind. Eng. Chem. Res.*, **53**, Nº 6, 2014, p. 2498-2508.